Realizing quantum gates with optically addressable $^{171}Yb^{+}$ ion qudits

M. A. Aksenov,[1,2] I. V. Zalivako,[1,2] I. A. Semerikov,[1,2] A. S. Borisenko,[1,2] N. V. Semenin,[1,2] P. L. Sidorov,[1,2] A. K. Fedorov,[2] K. Yu. Khabarova,[1,2] and N. N. Kolachevsky[1,2]

[1]*P. N. Lebedev Physical Institute of the Russian Academy of Sciences, Moscow 119991, Russia*

[2]*Russian Quantum Center, Skolkovo, Moscow 121205, Russia*

(Received 11 November 2022; revised 2 March 2023; accepted 8 May 2023; published 23 May 2023)

The use of multilevel information carriers, also known as qudits, is a promising path for exploring scalability of quantum computing devices. Here we present a proof-of-principle realization of a quantum processor register that uses optically addressed $^{171}Yb^{+}$ ion qudits in a linear trap. The rich level structure of $^{171}Yb^{+}$ ions allows using the Zeeman sublevels of the quadrupole clock transition at 435.5 nm for efficient and robust qudit encoding. We demonstrate the realization of the universal set of gates consisting of single-qudit rotations and a two-qudit Mølmer-Sørensen operation with a two-ququart system, which is formally equivalent to a universal gate-based four-qubit processor. Our results paves a way toward further studies of more efficient implementations of quantum algorithms with trapped-ion-based processors and, specifically, exploring properties of $^{171}Yb^{+}$ ion qudits.

DOI: 10.1103/PhysRevA.107.052612

I. INTRODUCTION

Quantum algorithms offer significant advantages over the best-known classical methods in solving certain computational problems ranging from prime factorization to simulating complex systems [1–5]. However, in order to run corresponding quantum algorithms in industry-relevant settings, one needs to operate with thousands of logical qubits [6,7], which cannot be provided by currently available quantum devices. The need for logical qubits requires sizable increase in fidelities of quantum gates, in particular, two-qubit operations. We note that the possibility to achieve computational advantage with noisy processors for practical problems remains questionable [8,9]. Recent progress in experiments with controllable quantum many-body systems based on superconducting circuits [10,11], semiconductor quantum dots [12–14], photonic systems [15,16], neutral atoms [17–20], and trapped ions [21–23] has made it possible to use such systems for tests on quantum advantage [10,11,15], quantum simulation [17–19,21,22], and prototyping quantum algorithms [20,23]. Although the reported numbers of qubits in quantum processors tend to hundreds (for example, 433-qubit superconducting quantum processor has been announced [24] and 256-atom quantum simulator has been used for optimization [25]), the reported gate fidelities of these large-scale processors are lower than in their small-scale counterparts [10,26]. Moreover, the connectivity between individual qubits is typically limited to their nearest neighbors, although there are various proposals to overcome this limitation [27]. These issues reduce the quantum volume (QV) [28] achieved by these devices, which is a metric for gate-based quantum processors combining the qubit number and gate fidelities.

Being one of the first platforms proposed for quantum computing [29,30], today trapped-ion systems show the highest QV of 32768 in experiments by Quantinuum with the 15-qubit H1-1 processor [31]. The trapped ion quantum processor also admits an effective error correction [32–37]; e.g., a fault-tolerant entanglement between two logical qubits has been realized [37,38]. Main features of trapped ions are long coherence times [39], high-fidelity gates [40], and essential all-to-all connectivity. Still, the scalability to large enough numbers of qubits without the decrease of the gate fidelities remains challenging [5,41].

An interesting feature of certain physical quantum platforms is their multilevel structure, which can be efficiently used for scaling quantum processors with the use of qudits—d-level quantum systems [42–81]. There are two basic approaches: (i) encoding several qubits in a single qudit and (ii) the use of additional qudit levels to substitute ancilla qubits in multiqubit gate decompositions [82] (for example, for the Toffoli gate [54,56,69,70,83–88]). These two methods can be efficiently combined [89]. Both approaches allow one to increase of the QV since a d-state qudit can be thought of as a $\log_2 d$ qubit. Additionally, certain two-qubit operations can be replaced by single-qudit ones. While the presence of additional energy levels is used for various quantum computing platforms [69,70,72–74,80,87,90], the use of qudit encoding is especially useful for trapped ions where switching from qubits to qudits is rather simple from an experimental point of view [66,91]. Notably, the first realization of two-qubit gates has used two qubits stored in the degrees of freedom of a single trapped ion, i.e., in the qudit setup [30].

Recently, multiqudit quantum processors [80,90,91], including the one based on $^{40}Ca^{+}$ qudits [91], have been demonstrated. In trapped-ion systems, quantum information is typically encoded in metastable states of ions, which are coupled by optical or microwave (mw) fields to perform quantum operations. In the case of using qudits, for example, the Zeeman structure of the 729-nm optical transition in $^{40}Ca^{+}$ ion has been used for the qudit encoding with d up to 7 [91]. One may argue that transition frequencies between certain of the sublevels are more susceptible to magnetic field

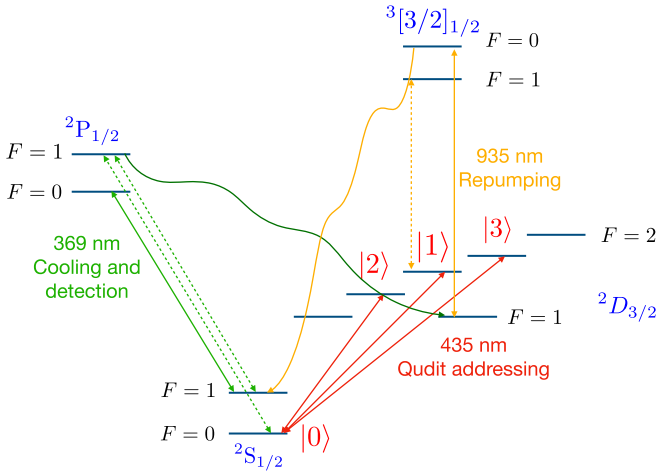

FIG. 1. $^{171}Yb^+$ level structure used for qudit manipulations: The state $|0\rangle$ is coupled to $|1\rangle$, $|2\rangle$, and $|3\rangle$ using single-qudit operations $R_{01}(\phi,\theta)$, $R_{02}(\phi,\theta)$, and $R_{03}(\phi,\theta)$, correspondingly. Arrows show laser fields used for the ion cooling and readout (green), repumping (orange), and quantum gates (red). Dotted arrows show fields generated by phase modulation of the laser beams, while curved lines correspond to spontaneous decays.

fluctuations in contrast to the one usually chosen as a qubit (see Fig. 1). However, with the proper magnetic shielding, one can significantly reduce the impact of the field noise on the coherence time. It is possible to realize a universal gate set consisting of single-qudit and two-qudit operations. However, finding best-possible conditions for developing scalable qudit-based quantum processors requires additional research. Specifically, another promising option for trapped-ion setups is to use $^{171}Yb^+$, which offers certain advantages [41]. In particular, the ytterbium ion level structure provides multiple options for encoding quantum information with a high degree of robustness with respect to decoherence [31,38,39].

In this work, we present a two-ququart quantum processor using $^{171}Yb^+$ ions with the quadrupole clock transition at 435.5 nm used for efficient qudit encoding. This transition is widely used in metrology [92–95], and it has been recently proposed for robust qubit encoding with ytterbium ions [96]. Here we extend this idea for encoding qudits. We demonstrate the realization of the full set of quantum gates required for implementing algorithms, which consists of single-qudit gates with fidelities ranges from 83% to 89% and the two-qubit operation with $65 \pm 4\%$ fidelity. We note that a single two-qudit Mølmer-Sørensen (MS) gate acting on $|0\rangle$ and $|1\rangle$ states in both ions is sufficient to complete a full two-ququart gate set. Although it is possible to add more two-qudit operations acting on other qudit states to the gate set, it is unnecessary from point of view of universality and would significantly complicate a calibration process.

II. OPTICAL $^{171}Yb^+$ QUDITS

$^{171}Yb^+$ ions are one of the main work horses in quantum metrology and quantum computing [41]. These ions are directly laser cooled with 369.5-nm emission on a strong quasicyclic $^2S_{1/2} \rightarrow {}^2P_{1/2}$ transition with repumping using $^2D_{3/2} \rightarrow {}^3[3/2]_{1/2}$ transition at 935.2 nm [97,98]. This process can be implemented with widely available semiconductor lasers and does not require frequency conversion. Since we are interested in $^{171}Yb^+$ isotope (the nuclear spin equals $I = 1/2$), one can realize isotope-selective trap loading with another readily available diode laser at 398.9 nm.

In particular, the transition between hyperfine components of the ground state $^2S_{1/2}(F = 0, m_F = 0) \rightarrow {}^2S_{1/2}(F = 1, m_F = 0)$ is widely used as a mw qubit. Its transition frequency is insensitive (to the first order) to the magnetic field fluctuations. The qubit can be readily initialized by optical pumping to the single Zeeman sublevel of the $^2S_{1/2}(F = 0)$ manifold. We note that entanglement of two logical qubits [38], the largest QV [31], and the record coherence times [39] have been demonstrated exactly with this type of mw qubit.

In our previous work [96], we have proposed the electric quadrupole transition $^2S_{1/2}(F{=}0, m_F{=}0) \rightarrow {}^2D_{3/2}(F{=}2, m_F = 0)$ in $^{171}Yb^+$ to encode an optical qubit. This transition has a wavelength of 435.5 nm and the natural linewidth of 3 Hz (the corresponding upper level life time equals $\tau =$ 53 ms). Such encoding combines already mentioned features of ytterbium ions with advantages of optical qubits, mainly in addressing. First, for addressing optical qubits, one can use lasers with visible-light wavelength range, whereas for addressing mw qubits ultraviolet lasers are typically required. This allows using more efficient optical components, for example, TeO_2 acousto-optical deflectors (AODs), which exhibit much larger scan range. Second, in order to perform a two-qubit operation on mw qubits, two non-co-propagating laser beams are required, while for optical qubits a single beam is enough. Moreover, in comparison with $^{40}Ca^+$ optical qubits, the proposed transition in $^{171}Yb^+$ ions exhibits two orders of magnitude smaller sensitivity to the magnetic field (52 Hz/μT at 500 μT field offset required for cooling in comparison to 5600 Hz/μT in $^{40}Ca^+$ ions), which leads to lower requirements for magnetic shielding. However, exploring these potential advantages of $^{171}Yb^+$ ions requires additional studies, which are beyond the scope of the present work.

Similarly to the calcium ions, one may realize optical qudits in $^{171}Yb^+$. All six Zeeman sublevels of both upper and lower levels can be used for the information encoding giving rise to qudits with $d = 6$ (see Fig. 1). However, $^{171}Yb^+$ qudits are potentially better protected from decoherence due to magnetic field fluctuations, since qudit levels have the integer full angular momentum number F, with $F = 0$ for the lower level. The $|0\rangle$ and $|1\rangle$ qubit states' energies are sensitive to the magnetic field only in the second order due to zero magnetic quantum numbers. Other qudit states can be decoupled from magnetic fields noise using decoupling techniques similar to what is presented in Ref. [99]; however, the demonstration of decoupling methods is a topic for further research beyond the scope of the present work. In our proof-of-principle demonstration, we use only four of six available states for ququart encoding ($d = 4$), as this system can be straightforwardly mapped to a conventional qubit-based processor by considering each ququart to encode two qubits.

A. Qudit gates

In the further discussion, the ququart states are denoted as $|0\rangle$, $|1\rangle$, $|2\rangle$, and $|3\rangle$ according to Fig. 1. We realize a

universal set of gates consisting of single-qudit operation and a single two-qudit gate. We perform single-qudit operations $R_{0k}(\phi,\theta)$ on a particular ion by applying laser pulses resonant to the transitions between corresponding qudit states. The corresponding operation matrices have the following form:

$$R_{01}(\phi,\theta)=\begin{pmatrix}\cos\left(\frac{\theta}{2}\right) & -ie^{-i\phi}\sin\left(\frac{\theta}{2}\right) & 0 & 0\\ -ie^{i\phi}\sin\left(\frac{\theta}{2}\right) & \cos\left(\frac{\theta}{2}\right) & 0 & 0\\ 0 & 0 & 1 & 0\\ 0 & 0 & 0 & 1\end{pmatrix}, \quad (1)$$

$$R_{02}(\phi,\theta)=\begin{pmatrix}\cos\left(\frac{\theta}{2}\right) & 0 & -ie^{-i\phi}\sin\left(\frac{\theta}{2}\right) & 0\\ 0 & 1 & 0 & 0\\ -ie^{i\phi}\sin\left(\frac{\theta}{2}\right) & 0 & \cos\left(\frac{\theta}{2}\right) & 0\\ 0 & 0 & 0 & 1\end{pmatrix}, \quad (2)$$

$$R_{03}(\phi,\theta)=\begin{pmatrix}\cos\left(\frac{\theta}{2}\right) & 0 & 0 & -ie^{-i\phi}\sin\left(\frac{\theta}{2}\right)\\ 0 & 1 & 0 & 0\\ 0 & 0 & 1 & 0\\ -ie^{i\phi}\sin\left(\frac{\theta}{2}\right) & 0 & 0 & \cos\left(\frac{\theta}{2}\right)\end{pmatrix}, \quad (3)$$

where $\theta=\Omega\tau_S$ (Ω is the Rabi frequency and τ_S is the laser pulse duration) and ϕ is the phase, which can be controlled by the laser field phase.

To entangle two particles, we use the well-known Mølmer-Sørensen gate [100–103] with $\pi/4$ phase. We apply this operation to $|0\rangle$ and $|1\rangle$ states of the neighboring ions, so further we denote it as $XX^{AB}_{01,01}(\pi/4)$. If we neglect additional phases gained by each of the qudits [91], as they can be compensated by a set of single-qudit operations, the gate can be described by the matrix:

$$XX^{AB}_{01,01}(\chi)=\exp(-i\chi\tilde{X}_{01}\otimes\tilde{X}_{01}),$$
$$\tilde{X}_{01}=\begin{pmatrix}0 & 1 & 0 & 0\\ 1 & 0 & 0 & 0\\ 0 & 0 & 0 & 0\\ 0 & 0 & 0 & 0\end{pmatrix}, \quad (4)$$

where χ is the phase. We note that $XX^{AB}_{01,01}(\pi/4)$ acting on $|00\rangle^{AB}$ leads to the generation of the Bell state having the following form:

$$|\Psi\rangle^{AB}=(|00\rangle^{AB}-i|11\rangle^{AB})/\sqrt{2}. \quad (5)$$

To perform the MS gate, we apply a bichromatic laser field with frequencies of $\omega_{01}\pm(\omega_m+\delta)$ onto both ions, where ω_{01} is the resonant frequency of the $|0\rangle\rightarrow|1\rangle$ transition, ω_m is the vibrational mode frequency used for entanglement, and δ is the detuning. To achieve the required gate phase, the pulse parameters must satisfy equation $\tau_{\rm MS}=2\pi/\delta=\pi/\eta\Omega$, where η is the Lamb-Dicke parameter for the selected mode and Ω is the resonant Rabi frequency of $|0\rangle\rightarrow|1\rangle$ transition. To entangle ions, we use the axial stretch mode with $\omega_m=2\pi\times809$ kHz. Axial modes are better spectrally separated from each other with respect to the radial ones; this enables one to neglect interactions with other modes. The stretch mode was chosen over the center-of-mass mode due to its higher frequency and lower sensitivity to heating, which reduces, first, the influence of the laser phase noise and, second, affect of ions anomalous heating on the gate fidelity. It can be shown (see, e.g., Ref. [91]) that this gate set, which consists of single-qudit operations and a two-qudit MS gate, is universal for this system.

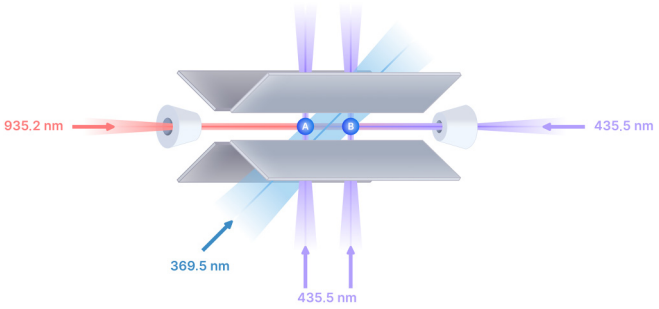

FIG. 2. The one-segment linear four-blade Paul trap is used for trapping $^{171}Yb^+$ ions (two ions are labeled as A and B). Laser beams shown in blue (369.5 nm) and red (935.2 nm) are used for Doppler cooling and repumping, respectively. The beam at 435.5 nm along the trap axis provides ground-state cooling and two-qubit gates. Another beam at 435.5 nm is orthogonal to the trap axis and its position can be tuned to address individual ions and perform single-qudit gates.

B. Qudit readout

The readout process for qudits is more complicated than for qubits, because more than two states should be distinguished. For a full readout of $^{171}Yb^+$ ion qudits, one may use the following approach. First, similarly to the usual electron shelving method [104], in order to project the ion onto $|0\rangle$ or a subspace spanned by other states we apply cooling and repumping laser (without modulation at 3.07 GHz) beams. This results in either strong fluorescence or its absence depending on the projection result, which can be distinguished with a photomultiplier tube (PMT) or an electron multiplying charge-coupled devices (EMCCD) camera. The population from $|0\rangle$ in this process is pumped to the $^2S_{1/2}(F=1)$ state. Then a $R_{0k}(0,\pi)$ gate is applied for transferring the population from $|k\rangle$ into $|0\rangle$, and the measurement is repeated. By performing the above procedure successively for each of the upper qudit states, the full readout is completed. For simplicity, one can omit reading out one of the states, as its population can be calculated from all the other measurements.

In order to reduce the degradation of the readout fidelity due to multiple imperfect single-qudit operations, we measure the population of only one state in each experimental run, and then repeat the experiment again to measure others. Using this approach, the probability to correctly distinguish $|0\rangle$ state from others is the same as for optical qubits [105]. For other states, it is reduced due to one additional single-qudit operation. We note that the used sequential readout method is not scalable, but it is useful for our proof-of-principle demonstration. Our plan is to switch to the first described readout method in the new version of our experimental setup.

III. TRAPPED-ION QUANTUM PROCESSOR WITH OPTICAL QUDITS

Here we describe our experimental setup for realizing a trapped-ion quantum processor with optical qudits. For trapping $^{171}Yb^+$ ions, we use an one-segment linear four-blade Paul trap with the secular frequencies of $\{\omega_x,\omega_y,\omega_z\}=2\pi\times\{1520,1500,467\}$ kHz (see Fig. 2). The upper levels' degeneracy is lifted up by applying a homogenous magnetic field of $B=500$ μT, which is also necessary for efficient laser cooling of $^{171}Yb^+$ ions by destabilization of the coherent

"dark states" [106]. The Zeeman splitting of the transition in this case appears to be 4.2 MHz. The magnetic field is produced by three pairs of orthogonally aligned coils with no special magnetic shielding.

We realize a two-particle ion string and use four states in each ion, $^2S_{1/2}(m_F = 0)$ and $^2D_{3/2}(m_F = 0, \pm 1)$, for encoding two ququarts, which we further refer to as qudit A and qudit B. At the beginning of each experimental run, ions are Doppler cooled for 5 ms, which brings the temperature of the ion crystal down to 1.7 mK [96]. Doppler cooling is achieved with diode lasers at 369.5 and 935.2 nm with electro-optical modulators (EOMs) at 14.7 and 3.07 GHz, respectively, to avoid population trapping in metastable hyperfine components. It is followed by qudit initialization to $|0\rangle$ by switching off the 14.7-GHz EOM and switching on the 2.1-GHz EOM installed in the 369.5-nm beam. The pumping process takes 5 μs.

Qudit manipulation on the quadrupole $^2S_{1/2}(F = 0, m_F = 0) \rightarrow {}^2D_{3/2}(F = 2, m_F = k)$ transitions is performed with a frequency doubled diode master-oscillator power-amplified laser system generating at fundamental wavelength of 871 nm. The oscillator is locked to a high-finesse external optical cavity made from ultra-low-expansion (ULE) glass providing the spectral linewidth of less than 30 Hz [95]. The linewidth was directly measured by spectroscopy of the qudit transition. The laser beam at 435.5 nm is split into two parts, one of which addresses ions globally along the trap axis and is used for two-qudit gates. The second part illuminates ions orthogonally to the trap axis and enables one to address ions individually. To address a particular ion, a pair of acousto-optic deflector (AOD) and acousto-optic modulator (AOM) is used. The former allows spatial scanning of the addressing beam through ions, while the latter is used for the beam frequency tuning and fast switching. We note that although the global addressing for entangling operations can be used for proof-of-principle demonstration, it prevents scaling of this system to larger number of ions. In following experiments, we plan to replace it with two individual addressing beams orthogonal to the trap axis and thus using radial modes of motion for particle entanglement. Although it requires more complex modulation of the addressing beams due to small spectral separation of radial modes, it is a well-established approach for scalable manipulation for systems of dozens of ions within the trap [107–110].

After the state initialization, a resolved-sideband technique [111] via $|0\rangle \rightarrow |1\rangle$ transition is used to achieve a ground-state cooling of both axial modes of ion motion. The mean number of phonons in the stretch mode, used for ions entanglement, achieves $n_{\mathrm{st}} = 0.079 \pm 0.013$.

The ground-state cooling is followed by the quantum operations themselves and readout. Ions fluorescence for readout is collected with a single aspheric lens which allows for individual ions resolving and is sent to the detector (PMT or EMCCD camera, depending on the experiment).

IV. REALIZATION OF THE SINGLE-QUDIT AND TWO-QUDIT GATES

Here we present results of proof-of-principle experiments with optical trapped ion qudits. We start with realizing single-qudit gates and estimating their performance. To estimate the fidelity of the single-qudit $R_{0k}(\phi, \theta)$ operations, we excite Rabi oscillations between $|0\rangle$ and $|k\rangle$ states for $k = 1, 2, 3$ with the pulse durations up to 200 μs (see Fig. 3). The resulting data are fitted with an exponentially damped sine function. The corresponding gate fidelity is estimated as the population of the $|k\rangle$ state in the first maximum, which is averaged over 300 measurements for each pulse duration.

TABLE I. Fidelities of single-qudit gates for two ion qudits. Operations were performed with two ions in the trap. Operation $2 \rightarrow 3$ is composed from three elementary ones.

	$0 \rightarrow 1$	$0 \rightarrow 2$	$0 \rightarrow 3$	$2 \rightarrow 3$
Qudit A	$\mathcal{F}^A_{01} = 85\%$	$\mathcal{F}^A_{02} = 83\%$	$\mathcal{F}^A_{03} = 87\%$	$\mathcal{F}^A_{23} = 65\%$
Qudit B	$\mathcal{F}^B_{01} = 87\%$	$\mathcal{F}^B_{02} = 89\%$	$\mathcal{F}^B_{03} = 87\%$	$\mathcal{F}^B_{23} = 70\%$

The fidelities for elementary single-qudit gates obtained with two qudits in the trap are presented in Table I; they range from 83% to 89%. At the moment our fidelities are limited by the temperature of the radial ion modes, which are not ground-state cooled. Readout errors also contribute to the estimated gate infidelities and, in particular, cause specious spectator qudit states excitations. The fidelity appears to be lower than in the optical qubit experiments (94%) reported in Ref. [96]. This can be explained by excessive heating of radial modes (above the Doppler limit) during the ground-state cooling of axial modes. After ground-state cooling of all vibrational modes in a next-generation setup, we expect the single-qudit fidelities to be at the same level as for $^{40}Ca^+$.

Nonpoint focusing of our optical addressing system leads to the excitation of the second ion while addressing the first one, which can be interpreted as a cross-talk. We measure the cross-talk by reading out the Rabi oscillations of one of the ions while exciting the other one by the laser field. The cross-talk turns out to be smaller than 10% and is due to the infidelity of the addressing optics. The discussion of the state preparation and measurement (SPAM) errors for our system in may be found in Ref. [96].

We also demonstrated the set composite of $R_{ik}(\phi, \theta)$ operations ($i, j = 1, 2, 3; i \neq j$) by applying consequential R_{0k} and R_{0i} pulses. The measured fidelity matches with what is expected to obtain from the corresponding product of each elementary operations.

Fidelity of the two-qudit operation was estimated by following Refs. [112,113], i.e., by measuring fidelity of the Bell state preparation. Two experiments were performed. In the first, we scan the duration of the bichromatic laser pulse for the entangling operation, after ions were initialized into $|00\rangle$. After that probabilities P_{00}, $P_{01} + P_{10}$, P_{11} of finding 0, 1, or 2 ions in the state $|1\rangle$ [see Fig. 4(b)] are measured. The optimal gate duration time manifests itself as the first dip in $P_{01} + P_{10}$. The magnitude of $P_{01} + P_{10} = 1 - \rho_{00,00} + \rho_{11,11}$ at this point characterizes the diagonal terms of the prepared state density matrix (here and after, $\rho_{ij,kl} = \mathrm{Tr}(\rho |i\rangle\langle j| \otimes |k\rangle\langle l|)$).

To estimate nondiagonal density matrix elements of the prepared Bell state, parity oscillations are measured. We apply $XX^{A,B}_{01,01}(\pi/4)$ gate with the optimal duration, after which the global $R_{01}(\phi, \pi/2)$ analyzing gate is performed. The

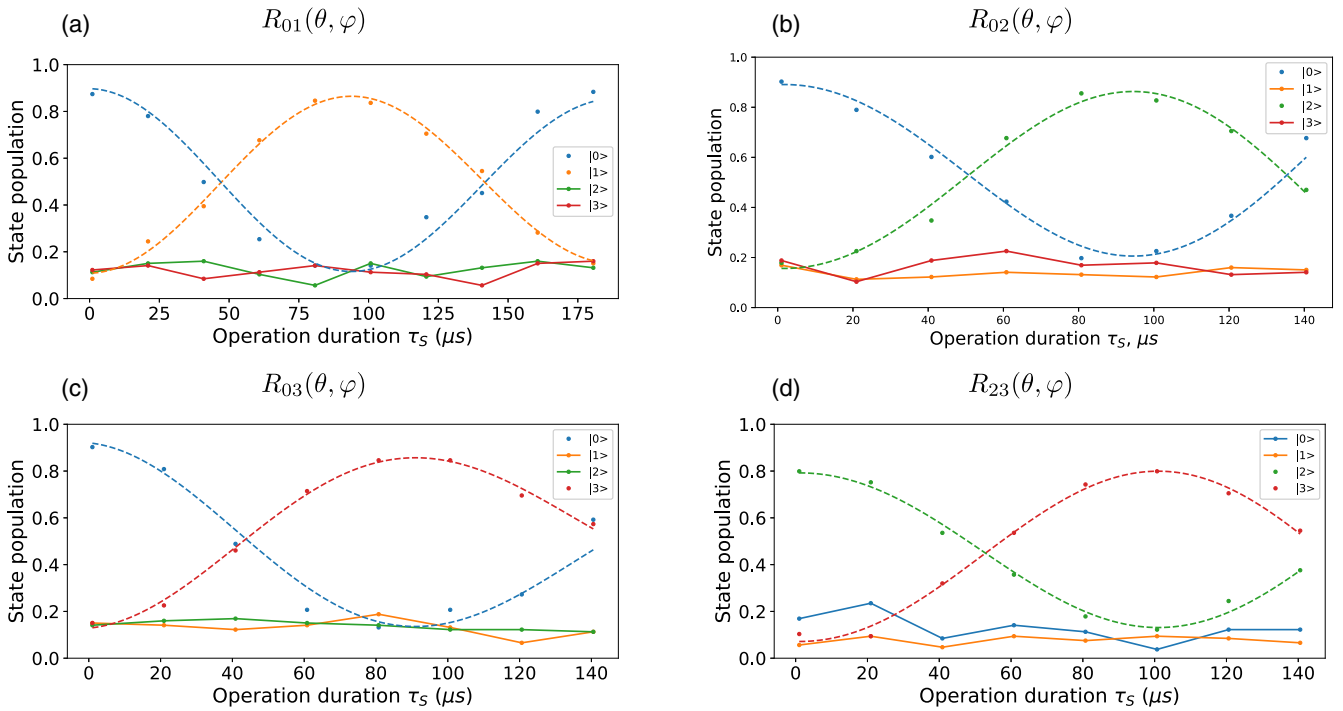

FIG. 3. Single-qudit gate realizations: dynamics of state populations when performing elementary single-qudit gates (a) $R_{01}(\theta,\varphi)$, (b) $R_{02}(\theta,\varphi)$, (c) $R_{03}(\theta,\varphi)$, and a composite gate (d) $R_{23}(\theta,\varphi)$ when gate duration $\tau_S \propto \theta$ is scanned. In the latter case, the ion was initially prepared into the $|2\rangle$ state by the π pulse on the $|0\rangle \rightarrow |2\rangle$ transition, after which a composite gate $R_{23}(\theta,\varphi) = R_{02}(\pi,\pi/2)R_{03}(\theta,\varphi)R_{02}(\pi,-\pi/2)$ followed.

dependency of the parity $P_a = P_{11} + P_{00} - P_{01} - P_{10} = 1 - 2(P_{01} - P_{10})$ on the analyzing pulse phase ϕ is measured [see Fig. 4(c)]. Fitting this dependence with function

$$P_a(\phi) = A \sin 2(\phi + \phi_0), \tag{6}$$

where A and ϕ_0 are free parameters, allows one to determine the coherence part of the prepared state density matrix as $|\rho_{00,11}| = A/2$.

The overall Bell-state preparation fidelity can be estimated as follows:

$$\begin{aligned}\mathcal{F}_{\text{Bell}} &= \langle \Psi^{AB}|\rho|\Psi^{AB}\rangle \\ &= (\rho_{00,00} + \rho_{11,11})/2 + |\rho_{00,11}|. \end{aligned} \tag{7}$$

Using such an estimation, we obtain $\mathcal{F}_{\text{MS}} = 65 \pm 4\%$ for two-qudit entanglement gate with the duration of $\tau_{\text{MS}} = 310$ μs. The main source of the two-qudit gate infidelity in our setup is the spectral phase noise of the addressing laser, which excite the carrier transition during the gate, and high

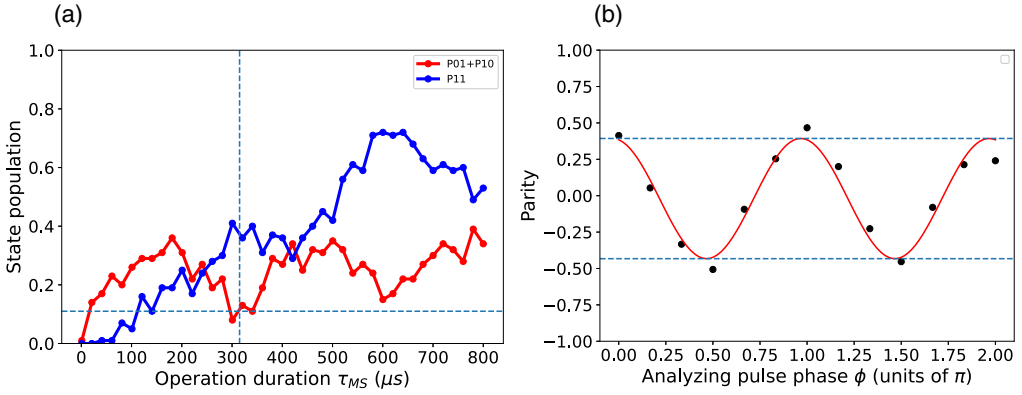

FIG. 4. Two-qudit gate realization: (a) probability of finding 1 ($P_{01} + P_{10}$) or 2 (P_{11}) ions in an excited state $|1\rangle$ after applying a bichromatic laser pulse of duration τ_{MS}; vertical dotted line shows τ_{MS} corresponding to $XX^{AB}_{01,01}(\pi/4)$ gate; (b) parity (6) oscillations $P_a(\phi)$ after applying a two-qudit gate $XX^{AB}_{01,01}(\pi/4)$ and analyzing gate $R^{AB}_{01}(\phi,\pi/2)$. Initially ions were prepared in $|00\rangle^{AB}$ state.

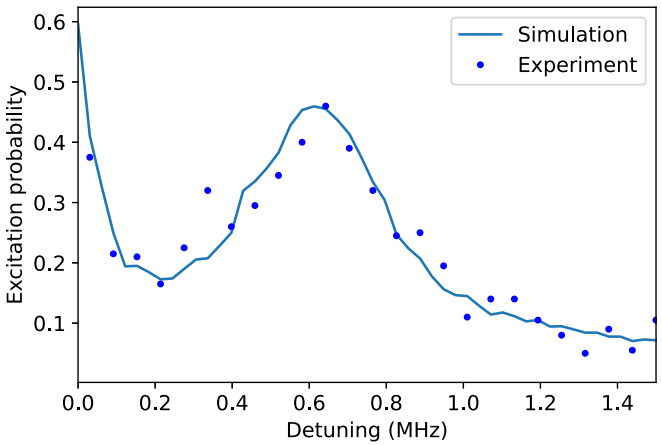

FIG. 5. Dependence of the $|0\rangle \rightarrow |1\rangle$ transition excitation probability on the laser detuning from the resonance (experimental data and simulation results). Rabi frequency is $\Omega = 2\pi \times 45$ kHz, laser pulse duration $\tau_p = 400\,\mu s$. As at detunings larger than $\Omega/2\pi$ excitation is mostly determined by the laser phase noise, fitting experimental data with a numeric model enables one to extract laser noise parameters.

heating rates of the trap. As we observe, the two-qudit gate fidelity strongly depends on the parameters of the lock of the addressing laser to the cavity. As the lock parameters determine the noise spectrum of the laser, we can assume that it has a leading contribution to the gate error.

To further validate this hypothesis, we performed a numeric simulation of the experiment including laser phase noise influence following [114]. To retrieve a laser noise power spectral density (PSD), ion spectroscopy was carried out on a $|0\rangle \rightarrow |1\rangle$ transition with an interrogating pulse duration much longer than a π pulse. Ion excitation at detunings larger than an on-resonance Rabi frequency is then determined by noise PSD at this detuning. Varying PSD in the numeric simulation and fitting experimental data with a simulated curve allows one to extract information about the laser phase noise. In Fig. 5, both measured spectrum and a simulated curve for optimized PSD parameters are shown. After that, extracted PSD data was used to simulate MS gate. The fidelity appeared to be on the level of 70%, which is close to experimentally observed results and proves laser noise to be the major contribution to the gate error. Thus, as we expect, existing shortcomings that prevent us from the demonstration of the state-of-the-art fidelities of quantum gates with ytterbium ions are of technical nature.

V. CONCLUSION AND OUTLOOK

We have presented the proof-of-principle realization of the two-ququarts quantum processor based on $^{171}Yb^+$ ions. Such a system is computationally analogous to a four-qubit processor and thus it may indicate on the potential advantages of the qudit approach to quantum computing. The qudits are encoded in the Zeeman structure of $^2S_{1/2}(F = 0)$ and $^2D_{3/2}(F = 2)$ levels, which are coupled via electric quadrupole transition at 435.5 nm. The system allows encoding qudits with d up to 6; however, in this demonstration only part of the available levels were used ($d = 4$). We have realized single-qudit and two-qudit gates, which constitute a universal gate set. The estimated fidelities of single-qudit gates range from 83% to 89% and of the two-qudit gate 65%. These fidelities are limited at the moment by the temperature of the ions and addressing laser phase noise. The results can be improved in our next generations of the setup, so we expect to reach the parameters regime reported in, e.g., in Ref. [91]. At the same time, the energy structure of the $^{171}Yb^+$ promises several advantages in developing decoherence-free qudit systems [99].

As we expect, with the increase in the number of qudits and fidelity of operations, qudit-based quantum processors will be able to demonstrate their advantages in realizing quantum algorithms in comparisons with their qubit-based counterparts. As has been shown in Ref. [89], the qudit-based realization provides an advantage both in the circuit width and depth. We would also like to note that the use of qudits, besides quantum computing, offers certain perspectives in quantum teleportation [65] and quantum communications [115,116], as well as opens up opportunities for uncovering fundamental concepts of quantum mechanics [58,62,117]. Thus, we expect that the future research on trapped ion qudits will be beneficial for various research avenues.

ACKNOWLEDGMENTS

We thank A. S. Nikolaeva, E. O. Kiktenko, and L. R. Bakker for fruitful discussions and useful comments. The experimental work was supported by Leading Research Center on Quantum Computing (Agreement No. 014/20) and Russian Roadmap on Quantum Computing (Contract No. 868-1.3-15/15-2021). The theoretical work of A.K.F. (analysis in Secs. II and IV) is also supported by the RSF Grant 19-71-10092.

[1] P. Shor, Algorithms for quantum computation: Discrete logarithms and factoring, in *Proceedings of the 35th Annual Symposium on Foundations of Computer Science* (1994), pp. 124–134

[2] S. Lloyd, Universal quantum simulators, Science **273**, 1073 (1996).

[3] A. W. Harrow, A. Hassidim, and S. Lloyd, Quantum Algorithm for Linear Systems of Equations, Phys. Rev. Lett. **103**, 150502 (2009).

[4] S. Lloyd, M. Mohseni, and P. Rebentrost, Quantum principal component analysis, Nat. Phys. **10**, 631 (2014).

[5] A. K. Fedorov, N. Gisin, S. M. Beloussov, and A. I. Lvovsky, Quantum computing at the quantum advantage threshold: A down-to-business review (2022).

[6] C. Gidney and M. Ekerå, How to factor 2048 bit RSA integers in 8 hours using 20 million noisy qubits, Quantum **5**, 433 (2021).

[7] M. Reiher, N. Wiebe, K. M. Svore, D. Wecker, and M. Troyer, Elucidating reaction mechanisms on quantum computers, Proc. Natl. Acad. Sci. USA **114**, 7555 (2017).

[8] M. Cerezo, A. Arrasmith, R. Babbush, S. C. Benjamin, S. Endo, K. Fujii, J. R. McClean, K. Mitarai, X. Yuan, L. Cincio,

and P. J. Coles, Variational quantum algorithms, Nat. Rev. Phys. **3**, 625 (2021).

[9] K. Bharti, A. Cervera-Lierta, T. H. Kyaw, T. Haug, S. Alperin-Lea, A. Anand, M. Degroote, H. Heimonen, J. S. Kottmann, T. Menke, W.-K. Mok, S. Sim, L.-C. Kwek, and A. Aspuru-Guzik, Noisy intermediate-scale quantum algorithms, Rev. Mod. Phys. **94**, 015004 (2022).

[10] F. Arute, K. Arya, R. Babbush, D. Bacon, J. C. Bardin, R. Barends, R. Biswas, S. Boixo, F. G. S. L. Brandao, D. A. Buell, B. Burkett, Y. Chen, Z. Chen, B. Chiaro, R. Collins, W. Courtney, A. Dunsworth, E. Farhi, B. Foxen, A. Fowler *et al.*, Quantum supremacy using a programmable superconducting processor, Nature (London) **574**, 505 (2019).

[11] Y. Wu, W.-S. Bao, S. Cao, F. Chen, M.-C. Chen, X. Chen, T.-H. Chung, H. Deng, Y. Du, D. Fan, M. Gong, C. Guo, C. Guo, S. Guo, L. Han, L. Hong, H.-L. Huang, Y.-H. Huo, L. Li, N. Li *et al.*, Strong Quantum Computational Advantage Using a Superconducting Quantum Processor, Phys. Rev. Lett. **127**, 180501 (2021).

[12] X. Xue, M. Russ, N. Samkharadze, B. Undseth, A. Sammak, G. Scappucci, and L. M. K. Vandersypen, Quantum logic with spin qubits crossing the surface code threshold, Nature (London) **601**, 343 (2022).

[13] M. T. Madzik, S. Asaad, A. Youssry, B. Joecker, K. M. Rudinger, E. Nielsen, K. C. Young, T. J. Proctor, A. D. Baczewski, A. Laucht, V. Schmitt, F. E. Hudson, K. M. Itoh, A. M. Jakob, B. C. Johnson, D. N. Jamieson, A. S. Dzurak, C. Ferrie, R. Blume-Kohout, and A. Morello, Precision tomography of a three-qubit donor quantum processor in silicon, Nature (London) **601**, 348 (2022).

[14] A. Noiri, K. Takeda, T. Nakajima, T. Kobayashi, A. Sammak, G. Scappucci, and S. Tarucha, Fast universal quantum gate above the fault-tolerance threshold in silicon, Nature (London) **601**, 338 (2022).

[15] H.-S. Zhong, H. Wang, Y.-H. Deng, M.-C. Chen, L.-C. Peng, Y.-H. Luo, J. Qin, D. Wu, X. Ding, Y. Hu, P. Hu, X.-Y. Yang, W.-J. Zhang, H. Li, Y. Li, X. Jiang, L. Gan, G. Yang, L. You, Z. Wang *et al.*, Quantum computational advantage using photons, Science **370**, 1460 (2020).

[16] L. S. Madsen, F. Laudenbach, M. F. Askarani, F. Rortais, T. Vincent, J. F. F. Bulmer, F. M. Miatto, L. Neuhaus, L. G. Helt, M. J. Collins, A. E. Lita, T. Gerrits, S. W. Nam, V. D. Vaidya, M. Menotti, I. Dhand, Z. Vernon, N. Quesada, and J. Lavoie, Quantum computational advantage with a programmable photonic processor, Nature (London) **606**, 75 (2022).

[17] S. Ebadi, T. T. Wang, H. Levine, A. Keesling, G. Semeghini, A. Omran, D. Bluvstein, R. Samajdar, H. Pichler, W. W. Ho, S. Choi, S. Sachdev, M. Greiner, V. Vuletić, and M. D. Lukin, Quantum phases of matter on a 256-atom programmable quantum simulator, Nature (London) **595**, 227 (2021).

[18] P. Scholl, M. Schuler, H. J. Williams, A. A. Eberharter, D. Barredo, K.-N. Schymik, V. Lienhard, L.-P. Henry, T. C. Lang, T. Lahaye, A. M. Läuchli, and A. Browaeys, Quantum simulation of 2d antiferromagnets with hundreds of Rydberg atoms, Nature (London) **595**, 233 (2021).

[19] L. Henriet, L. Beguin, A. Signoles, T. Lahaye, A. Browaeys, G.-O. Reymond, and C. Jurczak, Quantum computing with neutral atoms, Quantum **4**, 327 (2020).

[20] T. M. Graham, Y. Song, J. Scott, C. Poole, L. Phuttitarn, K. Jooya, P. Eichler, X. Jiang, A. Marra, B. Grinkemeyer, M. Kwon, M. Ebert, J. Cherek, M. T. Lichtman, M. Gillette, J. Gilbert, D. Bowman, T. Ballance, C. Campbell, E. D. Dahl *et al.*, Multi-qubit entanglement and algorithms on a neutral-atom quantum computer, Nature (London) **604**, 457 (2022).

[21] J. Zhang, G. Pagano, P. W. Hess, A. Kyprianidis, P. Becker, H. Kaplan, A. V. Gorshkov, Z. X. Gong, and C. Monroe, Observation of a many-body dynamical phase transition with a 53-qubit quantum simulator, Nature (London) **551**, 601 (2017).

[22] R. Blatt and C. F. Roos, Quantum simulations with trapped ions, Nat. Phys. **8**, 277 (2012).

[23] C. Hempel, C. Maier, J. Romero, J. McClean, T. Monz, H. Shen, P. Jurcevic, B. P. Lanyon, P. Love, R. Babbush, A. Aspuru-Guzik, R. Blatt, and C. F. Roos, Quantum Chemistry Calculations on a Trapped-Ion Quantum Simulator, Phys. Rev. X **8**, 031022 (2018).

[24] Our quantum road map is leading to increasingly larger and better chips, with a 1000-qubit chip, IBM Quantum Condor, targeted for the end of 2023, https://research.ibm.com/blog/ibm-quantum-roadmap

[25] S. Ebadi, A. Keesling, M. Cain, T. T. Wang, H. Levine, D. Bluvstein, G. Semeghini, A. Omran, J.-G. Liu, R. Samajdar, X.-Z. Luo, B. Nash, X. Gao, B. Barak, E. Farhi, S. Sachdev, N. Gemelke, L. Zhou, S. Choi, H. Pichler *et al.*, Quantum optimization of maximum independent set using Rydberg atom arrays, Science **376**, 1209 (2022).

[26] H. Levine, A. Keesling, A. Omran, H. Bernien, S. Schwartz, A. S. Zibrov, M. Endres, M. Greiner, V. Vuletić, and M. D. Lukin, High-Fidelity Control and Entanglement of Rydberg-Atom Qubits, Phys. Rev. Lett. **121**, 123603 (2018).

[27] D. Bluvstein, H. Levine, G. Semeghini, T. T. Wang, S. Ebadi, M. Kalinowski, A. Keesling, N. Maskara, H. Pichler, M. Greiner, V. Vuletic, and M. D. Lukin, A quantum processor based on coherent transport of entangled atom arrays Nature (London) **604**, 451 (2022).

[28] A. W. Cross, L. S. Bishop, S. Sheldon, P. D. Nation, and J. M. Gambetta, Validating quantum computers using randomized model circuits, Phys. Rev. A **100**, 032328 (2019).

[29] J. I. Cirac and P. Zoller, Quantum Computations with Cold Trapped Ions, Phys. Rev. Lett. **74**, 4091 (1995).

[30] C. Monroe, D. M. Meekhof, B. E. King, W. M. Itano, and D. J. Wineland, Demonstration of a Fundamental Quantum Logic Gate, Phys. Rev. Lett. **75**, 4714 (1995).

[31] Quantum volume reaches five digits for the first time: Five perspectives on what it means for quantum computing, https://www.quantinuum.com/news/quantum-volume-reaches-5-digits-for-the-first-time-5-perspectives-on-what-it-means-for-quantum-computing.

[32] J. Chiaverini, D. Leibfried, T. Schaetz, M. D. Barrett, R. B. Blakestad, J. Britton, W. M. Itano, J. D. Jost, E. Knill, C. Langer, R. Ozeri, and D. J. Wineland, Realization of quantum error correction, Nature (London) **432**, 602 (2004).

[33] P. Schindler, J. T. Barreiro, T. Monz, V. Nebendahl, D. Nigg, M. Chwalla, M. Hennrich, and R. Blatt, Experimental repetitive quantum error correction, Science **332**, 1059 (2011).

[34] R. Stricker, D. Vodola, A. Erhard, L. Postler, M. Meth, M. Ringbauer, P. Schindler, T. Monz, M. Müller, and R. Blatt, Experimental deterministic correction of qubit loss, Nature (London) **585**, 207 (2020).

[35] L. Egan, D. M. Debroy, C. Noel, A. Risinger, D. Zhu, D. Biswas, M. Newman, M. Li, K. R. Brown, M. Cetina, and C. Monroe, Fault-tolerant control of an error-corrected qubit, Nature (London) **598**, 281 (2021).

[36] A. Erhard, H. Poulsen Nautrup, M. Meth, L. Postler, R. Stricker, M. Stadler, V. Negnevitsky, M. Ringbauer, P. Schindler, H. J. Briegel, R. Blatt, N. Friis, and T. Monz, Entangling logical qubits with lattice surgery, Nature (London) **589**, 220 (2021).

[37] L. Postler, S. Heußen, I. Pogorelov, M. Rispler, T. Feldker, M. Meth, C. D. Marciniak, R. Stricker, M. Ringbauer, R. Blatt, P. Schindler, M. Müller, and T. Monz, Demonstration of fault-tolerant universal quantum gate operations, Nature (London) **605**, 675 (2022).

[38] C. Ryan-Anderson, N. C. Brown, M. S. Allman, B. Arkin, G. Asa-Attuah, C. Baldwin, J. Berg, J. G. Bohnet, S. Braxton, N. Burdick, J. P. Campora, A. Chernoguzov, J. Esposito, B. Evans, D. Francois, J. P. Gaebler, T. M. Gatterman, J. Gerber, K. Gilmore, D. Gresh *et al.*, Implementing fault-tolerant entangling gates on the five-qubit code and the color code, arXiv:2208.01863.

[39] P. Wang, C.-Y. Luan, M. Qiao, M. Um, J. Zhang, Y. Wang, X. Yuan, M. Gu, J. Zhang, and K. Kim, Single ion qubit with estimated coherence time exceeding one hour, Nat. Commun. **12**, 233 (2021).

[40] J. P. Gaebler, T. R. Tan, Y. Lin, Y. Wan, R. Bowler, A. C. Keith, S. Glancy, K. Coakley, E. Knill, D. Leibfried, and D. J. Wineland, High-Fidelity Universal Gate set for $^{9}Be^{+}$ Ion Qubits, Phys. Rev. Lett. **117**, 060505 (2016).

[41] C. D. Bruzewicz, J. Chiaverini, R. McConnell, and J. M. Sage, Trapped-ion quantum computing: Progress and challenges, Appl. Phys. Rev. **6**, 021314 (2019).

[42] E. Farhi and S. Gutmann, Analog analogue of a digital quantum computation, Phys. Rev. A **57**, 2403 (1998).

[43] A. R. Kessel and V. L. Ermakov, Multiqubit spin, J. Exp. Theor. Phys. Lett. **70**, 61 (1999).

[44] A. R. Kessel and V. L. Ermakov, Physical implementation of three-qubit gates on a separate quantum particle, J. Exp. Theor. Phys. Lett. **71**, 307 (2000).

[45] A. R. Kessel and N. M. Yakovleva, Implementation schemes in NMR of quantum processors and the Deutsch-Jozsa algorithm by using virtual spin representation, Phys. Rev. A **66**, 062322 (2002).

[46] A. Muthukrishnan and C. R. Stroud, Multivalued logic gates for quantum computation, Phys. Rev. A **62**, 052309 (2000).

[47] M. A. Nielsen, M. J. Bremner, J. L. Dodd, A. M. Childs, and C. M. Dawson, Universal simulation of hamiltonian dynamics for quantum systems with finite-dimensional state spaces, Phys. Rev. A **66**, 022317 (2002).

[48] X. Wang, B. C. Sanders, and D. W. Berry, Entangling power and operator entanglement in qudit systems, Phys. Rev. A **67**, 042323 (2003).

[49] A. B. Klimov, R. Guzmán, J. C. Retamal, and C. Saavedra, Qutrit quantum computer with trapped ions, Phys. Rev. A **67**, 062313 (2003).

[50] E. Bagan, M. Baig, and R. Muñoz-Tapia, Minimal measurements of the gate fidelity of a qudit map, Phys. Rev. A **67**, 014303 (2003).

[51] A. Y. Vlasov, Algebra of quantum computations with higher dimensional systems, in *First International Symposium on Quantum Informatics*, edited by Y. I. Ozhigov (SPIE, Lipki, Russian Federation, 2003), Vol. 5128, pp. 29–36.

[52] A. D. Greentree, S. G. Schirmer, F. Green, L. C. L. Hollenberg, A. R. Hamilton, and R. G. Clark, Maximizing the Hilbert Space for a Finite Number of Distinguishable Quantum States, Phys. Rev. Lett. **92**, 097901 (2004).

[53] D. P. O'Leary, G. K. Brennen, and S. S. Bullock, Parallelism for quantum computation with qudits, Phys. Rev. A **74**, 032334 (2006).

[54] T. C. Ralph, K. J. Resch, and A. Gilchrist, Efficient Toffoli gates using qudits, Phys. Rev. A **75**, 022313 (2007).

[55] B. P. Lanyon, T. J. Weinhold, N. K. Langford, J. L. O'Brien, K. J. Resch, A. Gilchrist, and A. G. White, Manipulating Biphotonic Qutrits, Phys. Rev. Lett. **100**, 060504 (2008).

[56] R. Ionicioiu, T. P. Spiller, and W. J. Munro, Generalized Toffoli gates using qudit catalysis, Phys. Rev. A **80**, 012312 (2009).

[57] S. S. Ivanov, H. S. Tonchev, and N. V. Vitanov, Time-efficient implementation of quantum search with qudits, Phys. Rev. A **85**, 062321 (2012).

[58] B. Li, Z.-H. Yu, and S.-M. Fei, Geometry of quantum computation with qutrits, Sci. Rep. **3**, 2594 (2013).

[59] E. O. Kiktenko, A. K. Fedorov, O. V. Man'ko, and V. I. Man'ko, Multilevel superconducting circuits as two-qubit systems: Operations, state preparation, and entropic inequalities, Phys. Rev. A **91**, 042312 (2015).

[60] E. Kiktenko, A. Fedorov, A. Strakhov, and V. Man'ko, Single qudit realization of the Deutsch algorithm using superconducting many-level quantum circuits, Phys. Lett. A **379**, 1409 (2015).

[61] C. Song, S.-L. Su, J.-L. Wu, D.-Y. Wang, X. Ji, and S. Zhang, Generation of tree-type three-dimensional entangled states via adiabatic passage, Phys. Rev. A **93**, 062321 (2016).

[62] A. Frydryszak, L. Jakóbczyk, and P. Ługiewicz, Determining quantum correlations in bipartite systems: From qubit to qutrit and beyond, J. Phys.: Conf. Ser. **804**, 012016 (2017).

[63] A. Bocharov, M. Roetteler, and K. M. Svore, Factoring with qutrits: Shor's algorithm on ternary and metaplectic quantum architectures, Phys. Rev. A **96**, 012306 (2017).

[64] P. Gokhale, J. M. Baker, C. Duckering, N. C. Brown, K. R. Brown, and F. T. Chong, Asymptotic improvements to quantum circuits via qutrits, in *Proceedings of the 46th International Symposium on Computer Architecture*, ISCA '19 (ACM Press, New York, 2019), pp. 554–566.

[65] Y.-H. Luo, H.-S. Zhong, M. Erhard, X.-L. Wang, L.-C. Peng, M. Krenn, X. Jiang, L. Li, N.-L. Liu, C.-Y. Lu, A. Zeilinger, and J.-W. Pan, Quantum Teleportation in High Dimensions, Phys. Rev. Lett. **123**, 070505 (2019).

[66] P. J. Low, B. M. White, A. A. Cox, M. L. Day, and C. Senko, Practical trapped-ion protocols for universal qudit-based quantum computing, Phys. Rev. Res. **2**, 033128 (2020).

[67] Z. Jin, W.-J. Gong, A.-D. Zhu, S. Zhang, Y. Qi, and S.-L. Su, Dissipative preparation of qutrit entanglement via periodically modulated Rydberg double antiblockade, Opt. Express **29**, 10117 (2021).

[68] M. Neeley, M. Ansmann, R. C. Bialczak, M. Hofheinz, E. Lucero, A. D. O'Connell, D. Sank, H. Wang, J. Wenner, A. N. Cleland, M. R. Geller, and J. M. Martinis, Emulation of a

quantum spin with a superconducting phase qudit, Science **325**, 722 (2009).

[69] B. P. Lanyon, M. Barbieri, M. P. Almeida, T. Jennewein, T. C. Ralph, K. J. Resch, G. J. Pryde, J. L. O'Brien, A. Gilchrist, and A. G. White, Simplifying quantum logic using higher-dimensional Hilbert spaces, Nat. Phys. **5**, 134 (2009).

[70] A. Fedorov, L. Steffen, M. Baur, M. P. da Silva, and A. Wallraff, Implementation of a Toffoli gate with superconducting circuits, Nature (London) **481**, 170 (2012).

[71] B. E. Mischuck, S. T. Merkel, and I. H. Deutsch, Control of inhomogeneous atomic ensembles of hyperfine qudits, Phys. Rev. A **85**, 022302 (2012).

[72] M. J. Peterer, S. J. Bader, X. Jin, F. Yan, A. Kamal, T. J. Gudmundsen, P. J. Leek, T. P. Orlando, W. D. Oliver, and S. Gustavsson, Coherence and Decay of Higher Energy Levels of a Superconducting Transmon Qubit, Phys. Rev. Lett. **114**, 010501 (2015).

[73] E. Svetitsky, H. Suchowski, R. Resh, Y. Shalibo, J. M. Martinis, and N. Katz, Hidden two-qubit dynamics of a four-level Josephson circuit, Nat. Commun. **5**, 5617 (2014).

[74] J. Braumüller, J. Cramer, S. Schlör, H. Rotzinger, L. Radtke, A. Lukashenko, P. Yang, S. T. Skacel, S. Probst, M. Marthaler, L. Guo, A. V. Ustinov, and M. Weides, Multiphoton dressing of an anharmonic superconducting many-level quantum circuit, Phys. Rev. B **91**, 054523 (2015).

[75] M. Kues, C. Reimer, P. Roztocki, L. R. Cortés, S. Sciara, B. Wetzel, Y. Zhang, A. Cino, S. T. Chu, B. E. Little, D. J. Moss, L. Caspani, J. Azaña, and R. Morandotti, On-chip generation of high-dimensional entangled quantum states and their coherent control, Nature (London) **546**, 622 (2017).

[76] C. Godfrin, A. Ferhat, R. Ballou, S. Klyatskaya, M. Ruben, W. Wernsdorfer, and F. Balestro, Operating Quantum States in Single Magnetic Molecules: Implementation of Grover's Quantum Algorithm, Phys. Rev. Lett. **119**, 187702 (2017).

[77] R. Sawant, J. A. Blackmore, P. D. Gregory, J. Mur-Petit, D. Jaksch, J. Aldegunde, J. M. Hutson, M. R. Tarbutt, and S. L. Cornish, Ultracold polar molecules as qudits, New J. Phys. **22**, 013027 (2020).

[78] A. Pavlidis and E. Floratos, Quantum-Fourier-transform-based quantum arithmetic with qudits, Phys. Rev. A **103**, 032417 (2021).

[79] P. Rambow and M. Tian, Reduction of circuit depth by mapping qubit-based quantum gates to a qudit basis, arXiv:2109.09902.

[80] Y. Chi, J. Huang, Z. Zhang, J. Mao, Z. Zhou, X. Chen, C. Zhai, J. Bao, T. Dai, H. Yuan, M. Zhang, D. Dai, B. Tang, Y. Yang, Z. Li, Y. Ding, L. K. Oxenløwe, M. G. Thompson, J. L. O'Brien, Y. Li *et al.*, A programmable qudit-based quantum processor, Nat. Commun. **13**, 1166 (2022).

[81] A. S. Nikolaeva, E. O. Kiktenko, and A. K. Fedorov, Decomposing the generalized toffoli gate with qutrits, Phys. Rev. A **105**, 032621 (2022).

[82] A. Barenco, C. H. Bennett, R. Cleve, D. P. DiVincenzo, N. Margolus, P. Shor, T. Sleator, J. A. Smolin, and H. Weinfurter, Elementary gates for quantum computation, Phys. Rev. A **52**, 3457 (1995).

[83] W.-Q. Liu, H.-R. Wei, and L.-C. Kwek, Low-Cost Fredkin Gate with Auxiliary Space, Phys. Rev. Appl. **14**, 054057 (2020).

[84] J. M. Baker, C. Duckering, and F. T. Chong, Efficient quantum circuit decompositions via intermediate qudits, in *2020 IEEE 50th International Symposium on Multiple-Valued Logic (ISMVL)* (IEEE, Miyazaki, Japan, 2020), pp. 303–308.

[85] E. O. Kiktenko, A. S. Nikolaeva, P. Xu, G. V. Shlyapnikov, and A. K. Fedorov, Scalable quantum computing with qudits on a graph, Phys. Rev. A **101**, 022304 (2020).

[86] W.-Q. Liu, H.-R. Wei, and L.-C. Kwek, Universal quantum multi-qubit entangling gates with auxiliary spaces, Adv. Quantum Technol. **5**, 2100136 (2022).

[87] A. Galda, M. Cubeddu, N. Kanazawa, P. Narang, and N. Earnest-Noble, Implementing a ternary decomposition of the Toffoli gate on fixed-frequency transmon qutrits, arXiv:2109.00558.

[88] X. Gu, J. Allcock, S. An, and Y.-X. Liu, Efficient multi-qubit subspace rotations via topological quantum walks, arXiv:2111.06534.

[89] A. S. Nikolaeva, E. O. Kiktenko, and A. K. Fedorov, Efficient realization of quantum algorithms with qudits, arXiv:2111.04384.

[90] A. D. Hill, M. J. Hodson, N. Didier, and M. J. Reagor, Realization of arbitrary doubly-controlled quantum phase gates, arXiv:2108.01652.

[91] M. Ringbauer, M. Meth, L. Postler, R. Stricker, R. Blatt, P. Schindler, and T. Monz, A universal qudit quantum processor with trapped ions, Nat. Phys. **18**, 1053 (2022).

[92] C. Tamm, D. Engelke, and V. Bühner, Spectroscopy of the electric-quadrupole transition $^2S_{1/2}(f=0)-{}^2D_{3/2}(f=2)$ in trapped $^{171}Yb^+$, Phys. Rev. A **61**, 053405 (2000).

[93] C. Lacroûte, M. Souidi, P.-Y. Bourgeois, J. Millo, K. Saleh, E. Bigler, R. Boudot, V. Giordano, and Y. Kersalé, Compact Yb optical atomic clock project: Design principle and current status, J. Phys.: Conf. Ser. **723**, 012025 (2016).

[94] J. Leute, N. Huntemann, B. Lipphardt, C. Tamm, P. B. R. Nisbet-Jones, S. A. King, R. M. Godun, J. M. Jones, H. S. Margolis, P. B. Whibberley, A. Wallin, M. Merimaa, P. Gill, and E. Peik, Frequency comparison of $^{171}Yb^+$ ion optical clocks at PTB and NPL via GPS PPP, IEEE Trans. Ultrason. Ferroelectr. Freq. Control **63**, 981 (2016).

[95] I. A. Semerikov, K. Y. Khabarova, I. V. Zalivako, A. S. Borisenko, and N. N. Kolachevsky, Compact transportable optical standard based on a single 171Yb+ ion ("ybis" project), Bull. Lebedev Phys. Inst. **45**, 337 (2018).

[96] I. V. Zalivako, I. A. Semerikov, A. S. Borisenko, M. D. Aksenov, K. Y. Khabarova, and N. N. Kolachevsky, Experimental study of the optical qubit on the 435-nm quadrupole transition in the $^{171}Yb+$ ion, JETP Lett. **114**, 59 (2021).

[97] I. Zalivako, I. Semerikov, A. Borisenko, V. Smirnov, P. Vishnyakov, M. Aksenov, P. Sidorov, N. Kolachevsky, and K. Khabarova, Improved wavelength measurement of 2s1/2 → 2p1/2 and 2d3/2 → 3[3/2]1/2 transitions in Yb+, J. Russ. Laser Res. **40**, 375 (2019).

[98] S. Ejtemaee, R. Thomas, and P. C. Haljan, Optimization of Yb^+ fluorescence and hyperfine-qubit detection, Phys. Rev. A **82**, 063419 (2010).

[99] C. H. Valahu, I. Apostolatos, S. Weidt, and W. K. Hensinger, Quantum control methods for robust entanglement of trapped ions, J. Phys. B: At. Mol. Opt. Phys. **55**, 204003 (2022).

[100] F. Schmidt-Kaler, H. Häffner, M. Riebe, S. Gulde, G. P. T. Lancaster, T. Deuschle, C. Becher, C. F. Roos, J. Eschner, and R. Blatt, Realization of the Cirac-Zoller controlled-NOT quantum gate, Nature (London) **422**, 408 (2003).

[101] K. Mølmer and A. Sørensen, Multiparticle Entanglement of Hot Trapped Ions, Phys. Rev. Lett. **82**, 1835 (1999).

[102] A. Sørensen and K. Mølmer, Quantum Computation with Ions in Thermal Motion, Phys. Rev. Lett. **82**, 1971 (1999).

[103] A. Sørensen and K. Mølmer, Entanglement and quantum computation with ions in thermal motion, Phys. Rev. A **62**, 022311 (2000).

[104] J. C. Bergquist, R. G. Hulet, W. M. Itano, and D. J. Wineland, Observation of Quantum Jumps in a Single Atom, Phys. Rev. Lett. **57**, 1699 (1986).

[105] N. V. Semenin, A. S. Borisenko, I. V. Zalivako, I. A. Semerikov, K. Y. Khabarova, and N. N. Kolachevsky, Optimization of the readout fidelity of the quantum state of an optical qubit in the ^{171}Yb+ ion, JETP Lett. **114**, 486 (2021).

[106] E. Arimondo, Coherent population trapping in laser spectroscopy, Prog. Opt. **35**, 257 (1996).

[107] S. Debnath, N. M. Linke, C. Figgatt, K. A. Landsman, K. Wright, and C. Monroe, Demonstration of a small programmable quantum computer with atomic qubits, Nature (London) **536**, 63 (2016).

[108] K. Wright, K. M. Beck, S. Debnath, J. M. Amini, Y. Nam, N. Grzesiak, J. S. Chen, N. C. Pisenti, M. Chmielewski, C. Collins, K. M. Hudek, J. Mizrahi, J. D. Wong-Campos, S. Allen, J. Apisdorf, P. Solomon, M. Williams, A. M. Ducore, A. Blinov, S. M. Kreikemeier *et al.*, Benchmarking an 11-qubit quantum computer, Nat. Commun. **10**, 5464 (2019).

[109] I. Pogorelov, T. Feldker, C. D. Marciniak, L. Postler, G. Jacob, O. Krieglsteiner, V. Podlesnic, M. Meth, V. Negnevitsky, M. Stadler, B. Höfer, C. Wächter, K. Lakhmanskiy, R. Blatt, P. Schindler, and T. Monz, Compact ion-trap quantum computing demonstrator, PRX Quantum **2**, 020343 (2021).

[110] R. Blümel, N. Grzesiak, N. Pisenti, K. Wright, and Y. Nam, Power-optimal, stabilized entangling gate between trapped-ion qubits, npj Quantum Inf. **7**, 147 (2021).

[111] C. Monroe, D. M. Meekhof, B. E. King, S. R. Jefferts, W. M. Itano, D. J. Wineland, and P. Gould, Resolved-Sideband Raman Cooling of a Bound Atom to the 3D Zero-Point Energy, Phys. Rev. Lett. **75**, 4011 (1995).

[112] D. Leibfried, B. DeMarco, V. Meyer, D. Lucas, M. Barrett, J. Britton, W. M. Itano, B. Jelenković, C. Langer, T. Rosenband, and D. J. Wineland, Experimental demonstration of a robust, high-fidelity geometric two ion-qubit phase gate, Nature (London) **422**, 412 (2003).

[113] J. Benhelm, G. Kirchmair, C. F. Roos, and R. Blatt, Towards fault-tolerant quantum computing with trapped ions, Nat. Phys. **4**, 463 (2008).

[114] H. Nakav, R. Finkelstein, L. Peleg, and N. Akerman, Effect of fast noise on the fidelity of trapped-ion quantum gates, Phys. Rev. A **107**, 042622 (2023).

[115] N. J. Cerf, M. Bourennane, A. Karlsson, and N. Gisin, Security of Quantum Key Distribution Using d-Level Systems, Phys. Rev. Lett. **88**, 127902 (2002).

[116] M. Mirhosseini, O. S. Magaña-Loaiza, M. N. O'Sullivan, B. Rodenburg, M. Malik, M. P. J. Lavery, M. J. Padgett, D. J. Gauthier, and R. W. Boyd, High-dimensional quantum cryptography with twisted light, New J. Phys. **17**, 033033 (2015).

[117] P. Horodecki, L. Rudnicki, and K. Życzkowski, Five open problems in quantum information theory, PRX Quantum **3**, 010101 (2022).